

SPECTROSCOPIC STUDIES OF THE SOLAR CORONA. IV. PHYSICAL PROPERTIES OF CORONAL STRUCTURE

JAGDEV SINGH

Indian Institute of Astrophysics, Bangalore 560034, India; jsingh@iiap.ernet.in

KIYOSHI ICHIMOTO AND TAKASHI SAKURAI

National Astronomical Observatory, 2-21-1, Ohsawa, Mitaka, Tokyo 181-85 88, Japan

AND

S. MUNEEER

Indian Institute of Astrophysics, Kodaikanal 624103, India; muni@iiap.ernet.in

Received 2002 March 20; accepted 2002 November 7

ABSTRACT

We obtained spectrographic observations of several coronal structures at the limb overlying the sunspot regions, simultaneously in the Fe xiv (5303 Å) and Fe x (6374 Å) emission lines on several days, and simultaneously in three coronal emission lines 6374 Å (Fe x), 10747 Å (Fe xiii), and 10798 Å (Fe xiii) on some other days. The slit width of 160 μm provided a spatial resolution of 4'' and a spectral resolution of 77 mÅ (Fe xiv), 128 mÅ (Fe x), and 291 mÅ (Fe xiii). The width and intensity of all these lines were computed using Gaussian fits to the observed line profiles. The FWHM of the emission lines increases at an average rate of 1.24 mÅ arcsec⁻¹ for Fe x, 0.29 mÅ arcsec⁻¹ for Fe xiii, and -0.66 mÅ arcsec⁻¹ for Fe xiv. These values are inversely correlated with the corresponding ionization temperature for these emission lines. We speculate that the FWHM of emission lines in coronal structures increases with height if the associated ionization temperature is less than 1.6 × 10⁶ K, with the gradient depending upon the ionization temperature of the line, while it decreases with height for lines whose ionization temperature is greater than 1.6 × 10⁶ K. It implies that it may not always be possible to interpret the observed increase in FWHM with height in terms of an increase in nonthermal velocity.

Subject headings: Sun: corona — techniques: spectroscopic

1. INTRODUCTION

The profiles of the forbidden emission lines in the coronal spectrum (e.g., the Fe x red line at 6374 Å and the Fe xiv green line at 5303 Å) contain information on the physical parameters such as temperature, turbulence, mass motion, and density of the source. The study of variations in line profiles as a function of height above the limb can give clues to the dynamical and physical nature of coronal structures and the ambient corona. The majority of existing observations are of two types: (i) in one emission line over a two-dimensional coronal region at a given time, and (ii) slit spectroscopy covering several lines.

The space-borne observations show that the emission lines from the transition region and corona are wider than the thermal Doppler width corresponding to the electron temperature (Doschek et al. 1976; Mariska, Feldman, & Doschek 1978). The excess width is called “nonthermal width,” or “nonthermal velocity” in terms of velocity. Many authors have interpreted this nonthermal component as due to mass motions by hydromagnetic waves (e.g., Hassler et al. 1990). Doschek & Feldman (2000) determined the nonthermal motions as a function of position in streamer regions from the FWHM of EUV spectral line profiles, under the assumption that the ion temperature is equal to the electron temperature of the streamer plasma, in the range of 20–40 km s⁻¹. Seely et al. (1997) reported that the turbulent velocity of EUV spectral lines decreased from about 22 km s⁻¹ at 30'' above the limb to less than 10 km s⁻¹ at 109'' above the limb, and that the ion temperatures were at least a factor of about 2.5 higher than the ionization

equilibrium temperatures. Hara & Ichimoto (1999) found that for the face-on loops, the FWHM of both the red and green lines increases toward the top of the loop, whereas the edge-on loops showed an increase in the red line width and a decrease in the green line width. They found this tendency from observations of moderately bright active region NOAA 7590. Here it may be noted that the observations in the Fe x, Fe xiv, and Ca xv (λ 5694 Å) lines were not simultaneous. Recently, Doschek et al. (2001) have determined the nonthermal motions as a function of height in polar coronal holes from the EUV spectral lines and found that the nonthermal motions sometimes, but not always, increase with height above the limb.

To determine the variations in physical and dynamical conditions in steady coronal structures with time, we have obtained line profiles over a two-dimensional coronal region in 6374 and 5303 Å coronal emission lines simultaneously for several hours on a number of days, and in 6374, 10747, and 10798 Å lines on some other days. In our earlier papers (Singh et al. 1999, 2002a), we have already studied variations in the FWHM of the red and green lines. Singh et al. (1999) studied the correlation between the FWHM and the line intensity. They used the line intensity as a proxy for the height above the limb and found that the FWHM of the red emission line increases with height and that of the green line decreases with height. Singh et al. (2002a) computed the gradients of the FWHM of these lines as a function of height for several different coronal structures, but their main interest was on time variability, and the number of samples was limited. In the present study we have made a thorough statistical study based on a larger sample of data. In the present

paper, we also analyzed the data obtained simultaneously in the red and infrared lines for a comparative study of the gradients of FWHM of these lines. Singh et al. (2002b) analyzed the same infrared spectral lines, but their goal was density diagnostics.

The present data are of steady coronal structures overlying sunspot regions, and during the period of observations the regions under study did not show any $H\alpha$ activity such as flares or eruptions, or any coronal activity such as enhanced emissions or fast structural changes. In this paper, based on the variations of widths of coronal emission lines as a function of height, we discuss coronal heating mechanisms and the existence of propagating Alfvén or acoustic waves in the corona.

2. OBSERVATIONS

Spectrographic observations of several coronal regions in the green and red emission lines were obtained simultaneously with the 25 cm coronagraph of the Norikura Solar Observatory on several days during the years 1997–1998. On some other days similar observations were made in three coronal emission lines, 6374 Å (Fe x), 10747 Å (Fe xii), and 10798 Å (Fe xiii) simultaneously. The coudé-type coronagraph provided us an image scale of $25'' \text{ mm}^{-1}$, and the 7 m focal length Littrow-type spectrograph gave a dispersion of 2.17 Å mm^{-1} in the third order (at the red line). By choosing different orders for different coronal emission lines, we could observe the 6374 Å line in the third order and the 5303 Å line in the fourth order simultaneously by using two separate CCD cameras. One of the cameras that has a 512×512 format with a pixel size of $13.5 \mu\text{m}$ was directly mounted at the Littrow focus and was used to take spectra around the red line. The other camera, which has a 1024×1024 format with a pixel size of $24 \mu\text{m}$, coupled with a 20 cm aperture and 8.86 m focal length Cassegrain telescope, was located in the beam diffracted from the grating, which over-spilled the Littrow mirror of the main spectrograph. This camera recorded the spectra around the green line. Similarly, we could utilize the Cassegrain telescope to obtain the red line spectra in the third order and the spectra of two infrared lines in the second order at the Littrow focus, simultaneously. The binned CCDs provided us a dispersion of 31.8 mÅ per pixel at the green line, 58.4 mÅ per pixel at the red line, and 121 mÅ per pixel at the infrared lines. However, the slit width of $160 \mu\text{m}$ that was used to make most of the observations restricted the spectral resolutions to 77, 128, and 291 mÅ for the green, red, and infrared emission lines, respectively, and the spatial resolution to $4''$. A typical exposure time was 10–20 s for the red and green lines, depending upon the sky conditions, and 40–70 s for the infrared lines. The green and red line spectra were recorded with the same exposure times. The required exposure time for the red line was shorter than for the infrared lines. Therefore, to maintain the simultaneity in observations, the exposures for the two CCD cameras were started at the same time and the camera for recording the red line spectrum waited to begin the next exposure until the exposure for the infrared spectrum was completed. The inclination of the glass block installed in front of the entrance slit was changed to obtain the spectra at different locations in the solar corona successively to build a two-dimensional image. One raster scan could be completed in 10–60 minutes, depending on the exposure time and the number of steps.

A typical raster scan consisted of 50 positions with a step size of $4''$ and covered a coronal region of $200'' \times 500''$.

3. DATA ANALYSIS

All the spectra were first corrected for the dark current, flat field, and scattered light component due to sky brightness. The top panel of Figure 1a shows a typical observed green coronal emission line profile, and the bottom panel shows the residual line profile after the correction due to the dark current, flat field, and sky component. A Gaussian fit was then made to the corrected emission line profile at each location of the observed coronal region to compute its peak intensity $I(\lambda_0)$, central wavelength (λ_0), and width (w) of the emission line defined by an expression $I(\lambda) = I(\lambda_0) \exp\{-1/2[(\lambda - \lambda_0)/\omega]^2\}$. The full width at half-maximum (FWHM) was calculated using $\text{FWHM} = 2(2 \ln 2)^{1/2} \omega$. The values of the FWHM thus derived were corrected for the instrumental effects using the relation $\text{FWHM}(\text{line}) = [\text{FWHM}(\text{observed})^2 - \text{FWHM}(\text{spectrograph})^2]^{1/2}$. The computed Gaussian curve for the residual data shown in the bottom panel of Figure 1a indicates a good fit. Figures 1b and 1c show typical observed profile, residual line profile, and a Gaussian fit for the red and infrared emission lines, respectively. The errors in the line parameters thus determined are negligibly small (Singh et al. 2002a, 2002b).

The parameters of the emission lines were then plotted as functions of spatial locations to obtain spectroheliograms in the green and red coronal lines. The heliograms, which have different scales due to differences in the focal lengths of the optics used to image the spectra, were rescaled and brought to the same spatial scale and dimension using the solar disk spectrum obtained with three fiducial marks. The top left and right panels of Figure 2 show the distributions of the red and green line intensities in logarithmic scale of an observed coronal region. (For the description of the two middle panels, see § 4.1.) The bottom-most two panels show the intensity distribution, in logarithmic scale, of the red and infrared lines of a coronal region observed on another day. In the same manner we have carried out analysis of the data on the red and infrared lines, grouping two lines at a time, namely, 6374 and 10747 Å, and 10747 and 10798 Å.

Most of the coronal fine structures are not radial and their physical properties such as temperature, density, magnetic field, nonthermal velocity, etc., vary from one place to another. Therefore, if we wish to study the variations in line parameters in the radial direction, most of the time we come across different coronal structures, and low line intensities in between make it difficult to investigate the structures radially. We, therefore, decided to study the FWHM variations with height by going along a coronal structure, as shown by the plus marks in Figure 2. We have avoided the locations where two different structures appear to overlap. The emission line intensity decreases by a large amount as we move away from the visible coronal structure. Hence, we may say that, in spite of integration along the line of sight, most of the contribution to the emission line profile comes from the selected coronal structure. Depending on the extent of coronal structures, 15–25 locations were selected on the red line image with a spatial resolution of $4''$ on a coronal structure. The corresponding locations in the other images as shown in Figure 2 were selected automatically by the software. The structure marked in the figure is almost radial.

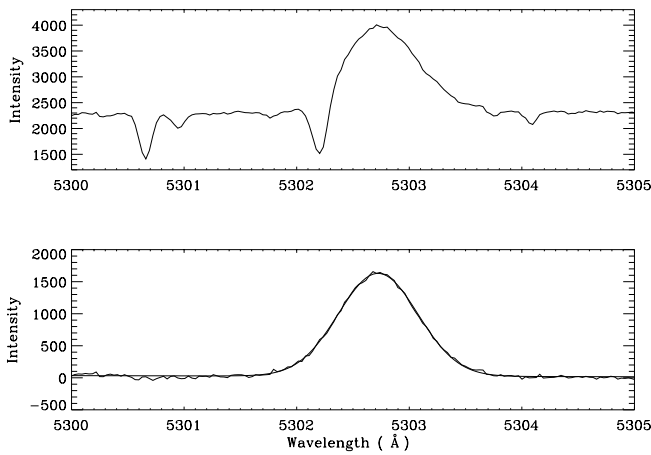


FIG. 1a

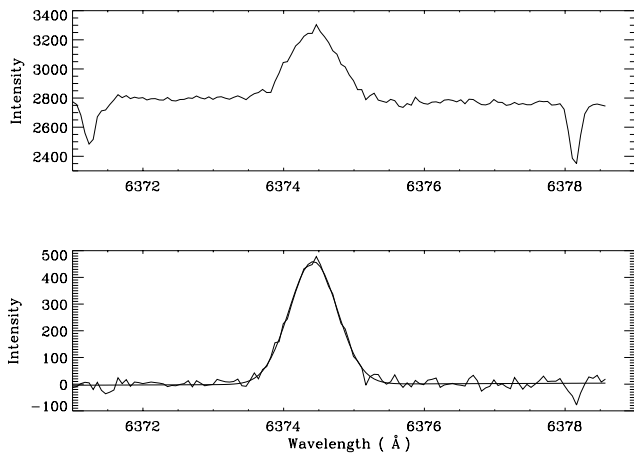


FIG. 1b

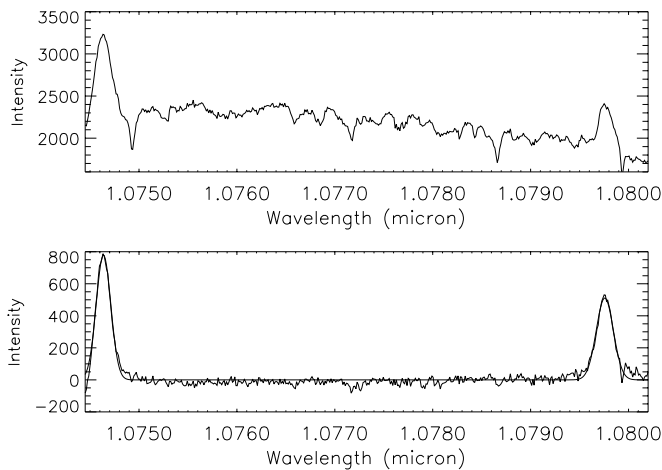


FIG. 1c

FIG. 1.—(a) Top panel shows a typical observed profile for the green coronal emission line (5303 Å). The residual profile after corrections for the dark frame, flat field, and scattered light due to sky brightness, and a Gaussian fit to the profile are shown in the bottom panel. (b) Same as (a), but for the red coronal emission line (6374 Å). (c) Same as (a), but for the two infrared emission lines at 10747 and 10798 Å.

To study the variation of the width of these lines with height above the limb, we determined the FWHM at various locations along the length of the individual structures. Most of the coronal structures showed sufficient intensity up to a

height of about 100'' above the limb. Therefore, we chose two representative heights, 50'' and 100'', to compare the line widths among different spectral lines and different structures. We computed the FWHM of the coronal emission lines at these two heights using a linear fit to the FWHM data as a function of height. Although we refer to the FWHM at 50'' or at 100'' in the following, these values were derived after the least-square fitting was made using many data points over the full height range of the observations.

4. RESULTS

A careful comparison of the red to green images, and red to infrared images, indicates that these images appear similar, respectively, although the fine structures do not overlap with each other exactly. The difference in the location of fine structures may be due to different temperatures and densities in different parts of the broad coronal structures. Also, some structures visible in the red image are not seen in the green image, and vice versa.

4.1. Green and Red Line Observations

There is a probability that different coronal structures contribute to the observed emission line profile because of integration along the line of sight. Some fine structures in the red and green line images (Fig. 2) appear similar, but they do not overlap exactly. Some others even look mutually exclusive. In order to study such situations quantitatively, we adopted the procedure as follows. First, we selected a structure in the red line image (case 1) as seen in the top panel of Figure 2, and the corresponding locations in the green line image were selected automatically by the software. To compare, we selected the nearby similar structure in the green line image (case 2), and the corresponding locations in the red line image were determined automatically, as shown in the middle panel of Figure 2. We always found some (if very weak) emission of the red line where the green line structure exits, or vice versa.

The top panel of Figure 3a (case 1) shows a plot of the green line intensity versus red line intensity. The middle panel shows a plot of the FWHM of the green (*triangles*) and red (*asterisks*) lines as a function of height, along with least-square linear fits to the respective data sets. The bottom panel shows the ratio of the green line intensity (I_g) to the red line intensity (I_r) versus height. Figure 3b is similar to 3a but was made for case 2. Both of these figures are similar and show that the FWHM of the green line decreases while that of the red line increases with height. The difference in these figures is that the line intensity ratio (I_g/I_r) is larger for case 2 than for case 1. This is because we started from the green line structure in case 2, and we tend to pick up a structure more prominent in the green line image.

The middle panel of Figure 3a indicates that the FWHM gradient for the green line is $-1.76 \text{ mÅ arcsec}^{-1}$ and that for the red line is $1.17 \text{ mÅ arcsec}^{-1}$. The exact values for the gradient might depend upon the geometry of the structure studied, but the general trend in the variation with height remains the same in all types of structures. To compare the most probable values of FWHM gradients for different emission lines, we have derived them from the linear fits to the data of 130 coronal structures. The frequency distribution of the FWHM gradients for the green and red lines is shown in Figure 4. The coronal structures considered are

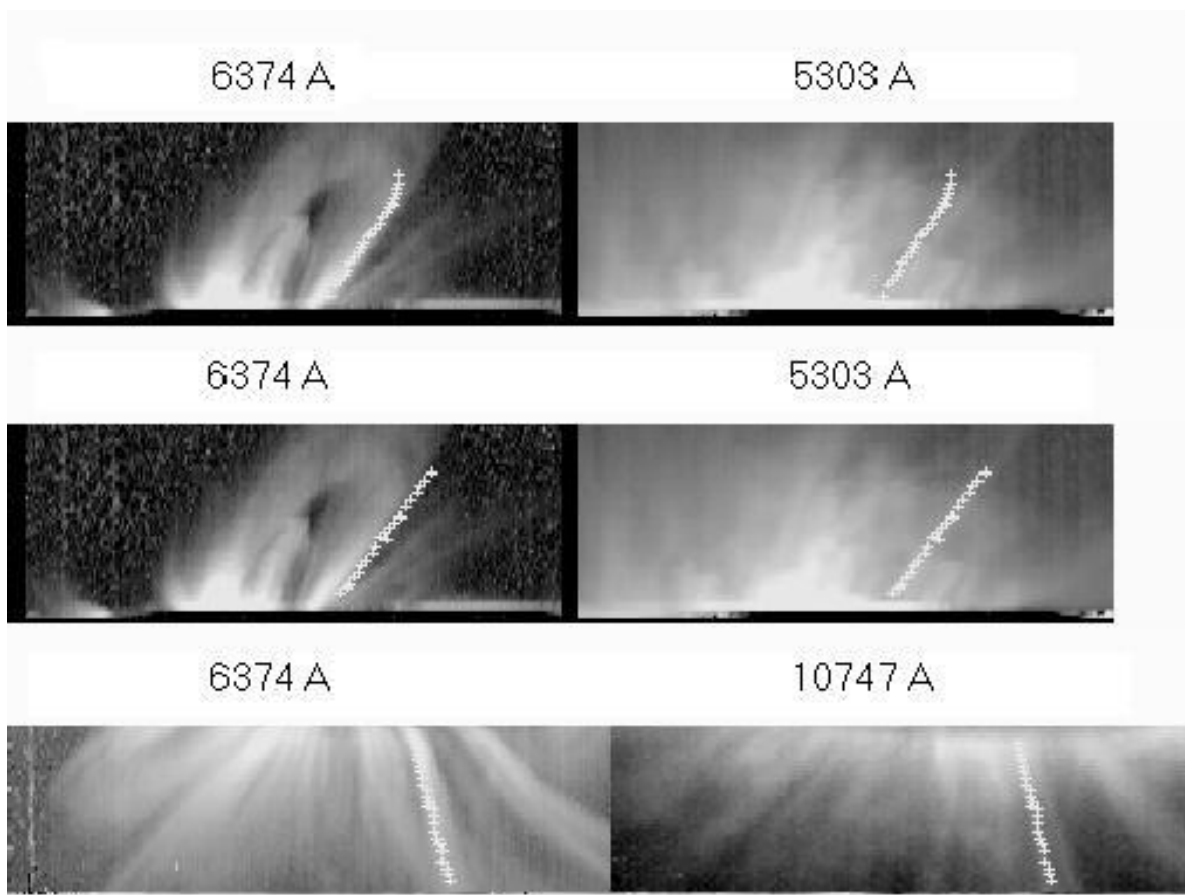


FIG. 2.—Top panel shows the spectroheliograms in the red and green emission lines observed on 1998 July 19. The relative intensity distribution is in logarithmic scale, with ranges 1.3–3.0, 1.5–3.3, and 1.1–2.5 for the red, green, and infrared lines, respectively. The red line image was displayed to emphasize a coronal structure. Locations marked by a plus sign along a coronal structure were selected to generate Fig. 3a. The middle panel shows the locations when the green line image was displayed to generate Fig. 3b. The bottom panel shows the structure in the red and infrared (10747 Å) lines observed on 1998 September 10. Locations marked by a plus sign in both images indicate that the structure is cospatial.

the same for both of these lines. We would expect a similar frequency distribution of the FWHM gradients with a marginal difference due to the differences in wavelengths of these lines, if we assume that an increase in FWHM is caused by either nonthermal velocity or temperature that increases with height. On the contrary, Figure 4 shows that 89% of the structures have a negative gradient for the green line and 95% of the structures have a positive gradient for the red line. The most probable value of the FWHM gradient for the green line is $-0.66 \text{ m\AA arcsec}^{-1}$ and that for the red line is $1.1 \text{ m\AA arcsec}^{-1}$.

To determine the most probable values of FWHM at certain heights and compute the representative nonthermal velocity, we have plotted in Figure 5 the frequency distribution of the FWHM at 50'' and 100'' for both the green and red lines. The figure shows that the most probable value of the FWHM of the green line at 50'' is 810 mÅ, and 765 mÅ at 100''. The corresponding values for the red line are 830 and 860 mÅ, respectively. The mean values of the FWHM and FWHM gradient are given in Table 1.

4.2. Red and Infrared Line Observations

To study the variation in the FWHM of the red and infrared lines, we adopted a procedure similar to that adopted for the study of the red and green line data. The bottom panel of Figure 2 shows that most of the structures in the

red and infrared lines are cospatial, but the intensity distribution in the two lines is not exactly the same. This may be because different structures have different physical properties.

The frequency distribution of the FWHM gradient of the red and infrared lines shown in Figure 4 indicates that 96% of the individual structures observed in the red line show a positive gradient with a mean value of $0.89 \text{ m\AA arcsec}^{-1}$, whereas only 57% of the structures observed in the 10747 Å

TABLE 1
MEAN VALUES OF FWHM (Å) AND ITS GRADIENTS (IN m\AA arcsec^{-1})
OF CORONAL EMISSION LINES

Emission Line	FWHM (50'')	FWHM (100'')	FWHM Gradient	FWHM Gradient/ λ
For the Red and Green Lines				
Green.....	0.822 ± 0.049	0.789 ± 0.063	-0.66	-1.25 ± 10^{-4}
Red.....	0.843 ± 0.050	0.905 ± 0.082	1.24	1.94 ± 10^{-4}
For the Red and Infrared Lines				
10747 Å.....	1.874 ± 0.099	1.886 ± 0.140	0.22	0.20 ± 10^{-4}
10798 Å.....	1.890 ± 0.107	1.912 ± 0.112	0.36	0.33 ± 10^{-4}
Red.....	0.868 ± 0.046	0.917 ± 0.061	0.98	1.54 ± 10^{-4}

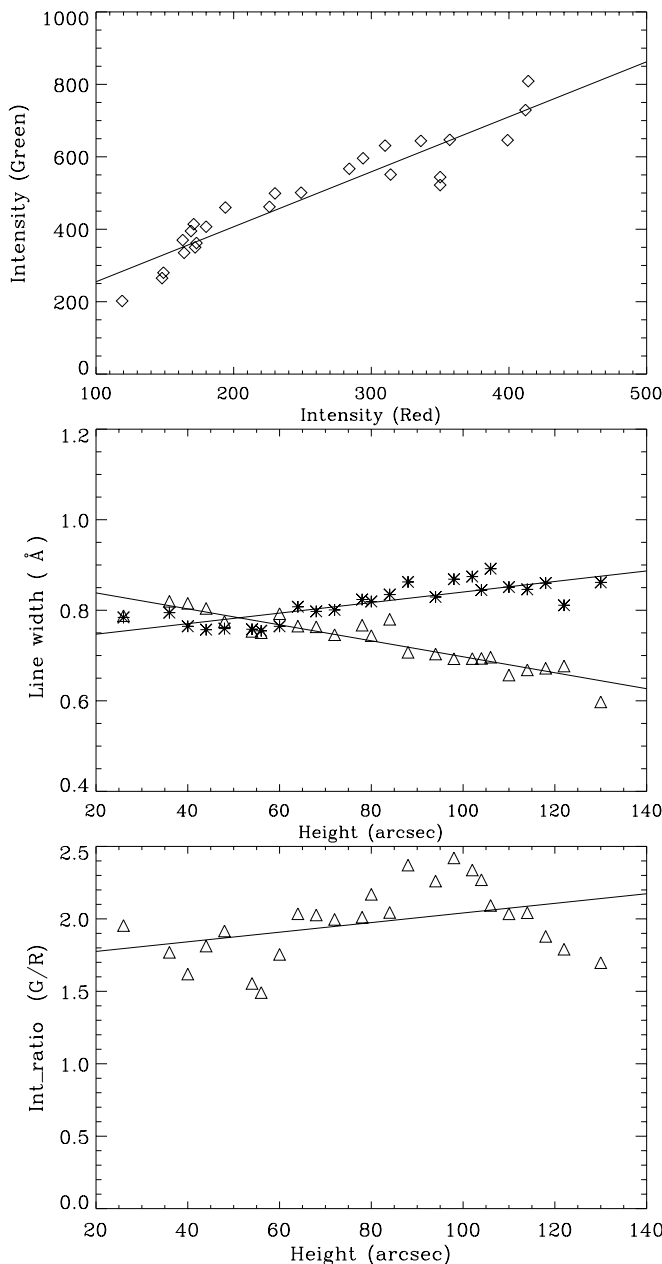


FIG. 3a

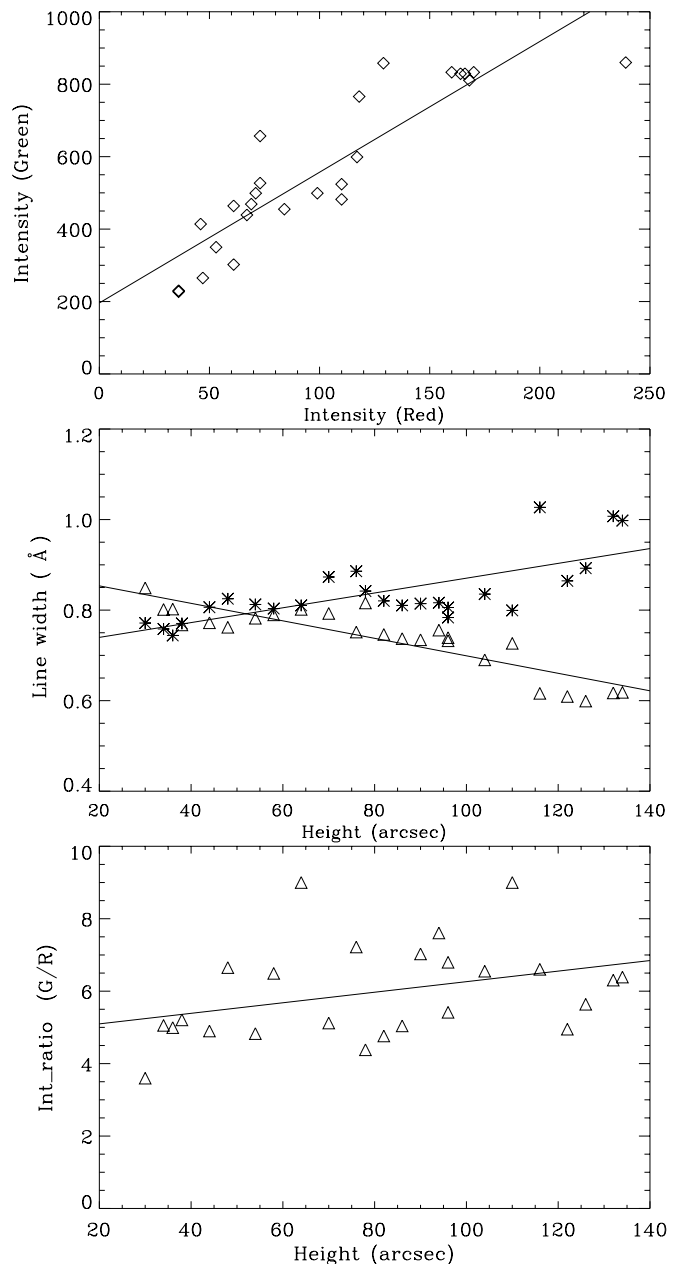


FIG. 3b

FIG. 3.—(a) Typical plot made after computing the values of line width and intensity over a $4'' \times 4''$ coronal region by displaying the red line image to select the locations. The top panel shows variation of the green line intensity vs. the red line intensity. The middle panel represents the FWHM of the green (*triangles*) and red line (*asterisks*) as a function of height above the limb along with linear fits (*straight lines*) to respective data sets. The bottom panel indicates the ratio of green to red line intensity vs. height above the solar limb. (b) Same as (a), but made by displaying the green line image to emphasize the locations.

line and 59% of those observed in the 10798 \AA line show a positive gradient with comparatively small mean values of 22 and $36 \text{ m\AA arcsec}^{-1}$, respectively. The mean values of the FWHM at $50''$ and $100''$ are also given in Table 1. The mean value of the FWHM of the 10798 \AA line is larger by 1.1% than that of the 10747 \AA line. A difference in dispersion at these two lines has been taken into account. The temperature of coronal structures for these two infrared lines can be defined as $T = (\text{FWHM}/\lambda)^2 \times \text{constant}$. If the temperature is the same for the two lines, one would expect the FWHM of the 10798 \AA line to be larger by about 0.5% than that of the 10747 \AA line. The remaining difference of 0.6% in FWHM of the two lines is still a puzzle to us how to interpret.

5. DISCUSSION

We found that the FWHM of the green line in most of the coronal structures decreases with height with a mean gradient of $-0.66 \text{ m\AA arcsec}^{-1}$, whereas the FWHM of the red line increases with height in most of the structures with a mean gradient of $1.1 \text{ m\AA arcsec}^{-1}$. The FWHM of the two infrared lines decreases with height for about 42% of the coronal structures and increases in the remaining structures. The mean value of the FWHM gradient is $0.29 \text{ m\AA arcsec}^{-1}$.

The variation in the FWHM of the coronal emission lines due to changes in temperature or nonthermal velocity in coronal structures will be proportional to the wavelength of

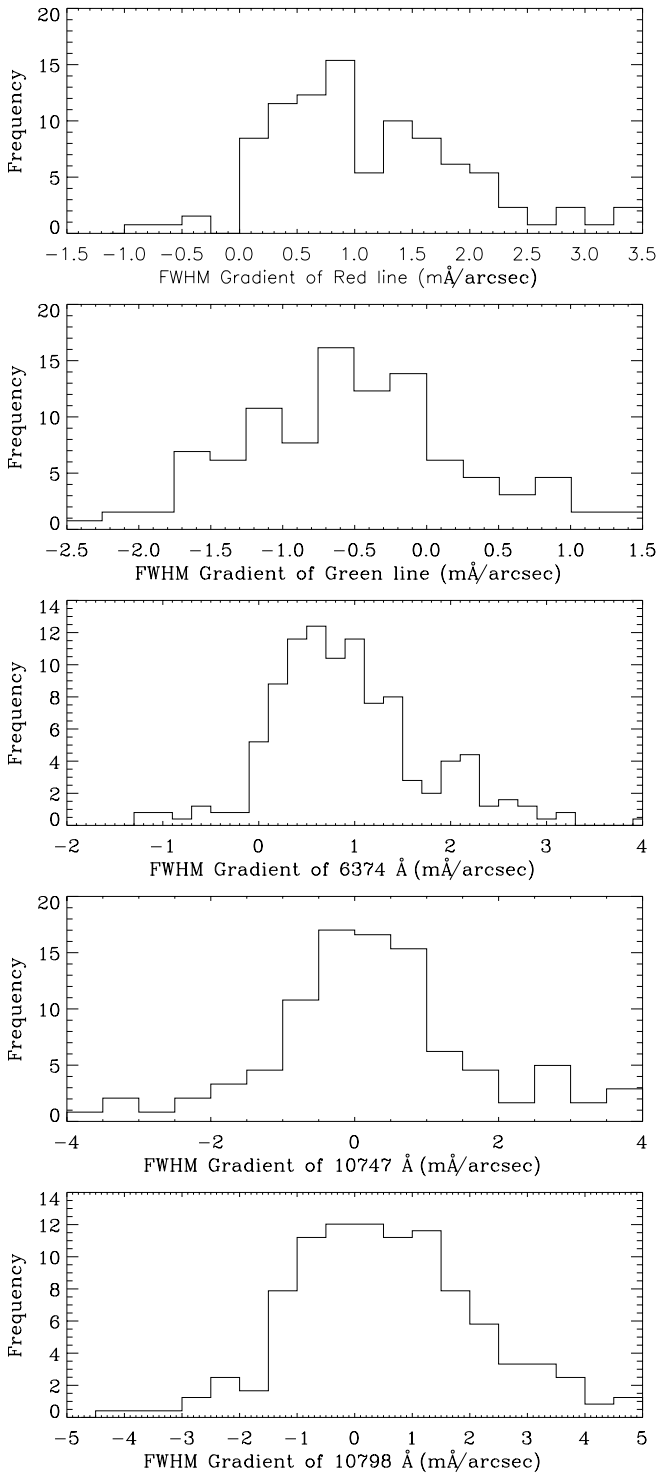


FIG. 4.—Frequency distribution of FWHM gradient for the green and red coronal emission lines made by combining all the observations obtained on different days is shown in the top two panels. The bottom three panels are for the red and infrared lines observed on some other days.

the emission line. The last column of Table 1 lists the mean values of the FWHM gradients normalized to the wavelength (its unit is arcsec^{-1}) for all the coronal emission lines. These values indicate that the change in FWHM/λ for the infrared lines is smaller than that for the green and red lines. The mean value (magnitude) of the $\text{FWHM gradient}/\lambda$ for

the green line is about 5 times, and for the red line is 7 times, that for the infrared lines.

The average FWHM values of the green, infrared, and red lines at $50''$ above the limb are 0.822 , 1.882 , and 0.856 Å, respectively. Assuming that the line widths are entirely due to thermal broadening, the temperatures corresponding to these values are appreciably higher than the ionization equilibrium temperatures, which are 1.8×10^6 , 1.6×10^6 , and 1.1×10^6 K, respectively (Arnaud & Rothenflug 1985).

We found that the average intensity ratio of the green to the red line is about 5.6 at $50''$ and 4.8 at $100''$. Those values correspond to temperatures of 1.52×10^6 and 1.50×10^6 K, respectively (Raju & Singh 1987). The use of two different values of these temperatures at $50''$ and $100''$ does not change the values of nonthermal velocities significantly. Therefore, we have assumed 1.5×10^6 K as the average temperature of the observed coronal structures to derive the nonthermal velocity, V_t , using the following equation $2kt/M + V_t^2 = (1/4 \ln 2)c^2\Delta\lambda^2/\lambda^2$, where T is the coronal temperature, M is the mass of the ion, c is the velocity of light, $\Delta\lambda$ is the full width at half-maximum, and λ is the wavelength of the coronal emission line. The computed values of nonthermal velocities for the green, infrared and red lines are 18.4 , 23.4 , and 11.9 km s^{-1} at $50''$, and 16.5 , 24.0 and 14.8 km s^{-1} at $100''$. For comparison, we have derived the values of nonthermal velocities assuming respective ionization equilibrium temperature for these emission lines. We find nonthermal velocities of 17.0 , 22.8 , and 15.8 km s^{-1} at $50''$ for the red, infrared, and green lines, respectively, and those at $100''$ are 19.2 , 23.1 , and 13.7 km s^{-1} . These values indicate that the nonthermal velocity increases in case of the red line, marginally increases in case of the infrared lines, and decreases in case of the green line. This kind of behavior in the change of the FWHM with height for these coronal emission lines indicates that the FWHM gradient is related to the temperature of the plasma in the structure; it is negative for a high temperature line, positive for a relatively low temperature line, and nearly zero for an intermediate temperature line.

If we assume that the nonthermal velocities increase in a coronal structure with height as concluded by Doyle, Banerjee, & Perez (1998), the width of all these lines also should increase with height. An increase of 56 mÅ in the FWHM of the red line at $100''$ from that at $50''$ corresponds to an increase of 3 km s^{-1} in the nonthermal velocity. This increase in the nonthermal velocity should cause an increase in the FWHM of the infrared lines by 137 mÅ at $100''$ from its value at $50''$, but the observed increase is only 15 mÅ. Further, the FWHM of the green line is smaller at $100''$ than that at $50''$. It should have been larger if the nonthermal velocity had been increased. Similarly, a monotonic increase or decrease in temperature within coronal structures with height also cannot account for a simultaneously observed increase in FWHM of the red line, marginal increase in FWHM of the infrared lines, and decrease in the FWHM of the green line with height. Hassler et al. (1990) and others have observed an increase in width of the emission lines, which they interpreted in terms of the existence of hydro-magnetic waves or Alfvén waves.

Doyle, Banerjee, & Perez (1998) found an increase of about 0.02 Å in the FWHM of the Si VIII line pair at 1445.75 and 1440.49 Å over a height of $35''$ above the limb. The gradient of the FWHM scaled to the wavelength is 3.9 mÅ arcsec^{-1} , which is larger than our mean value of 1.74 mÅ for

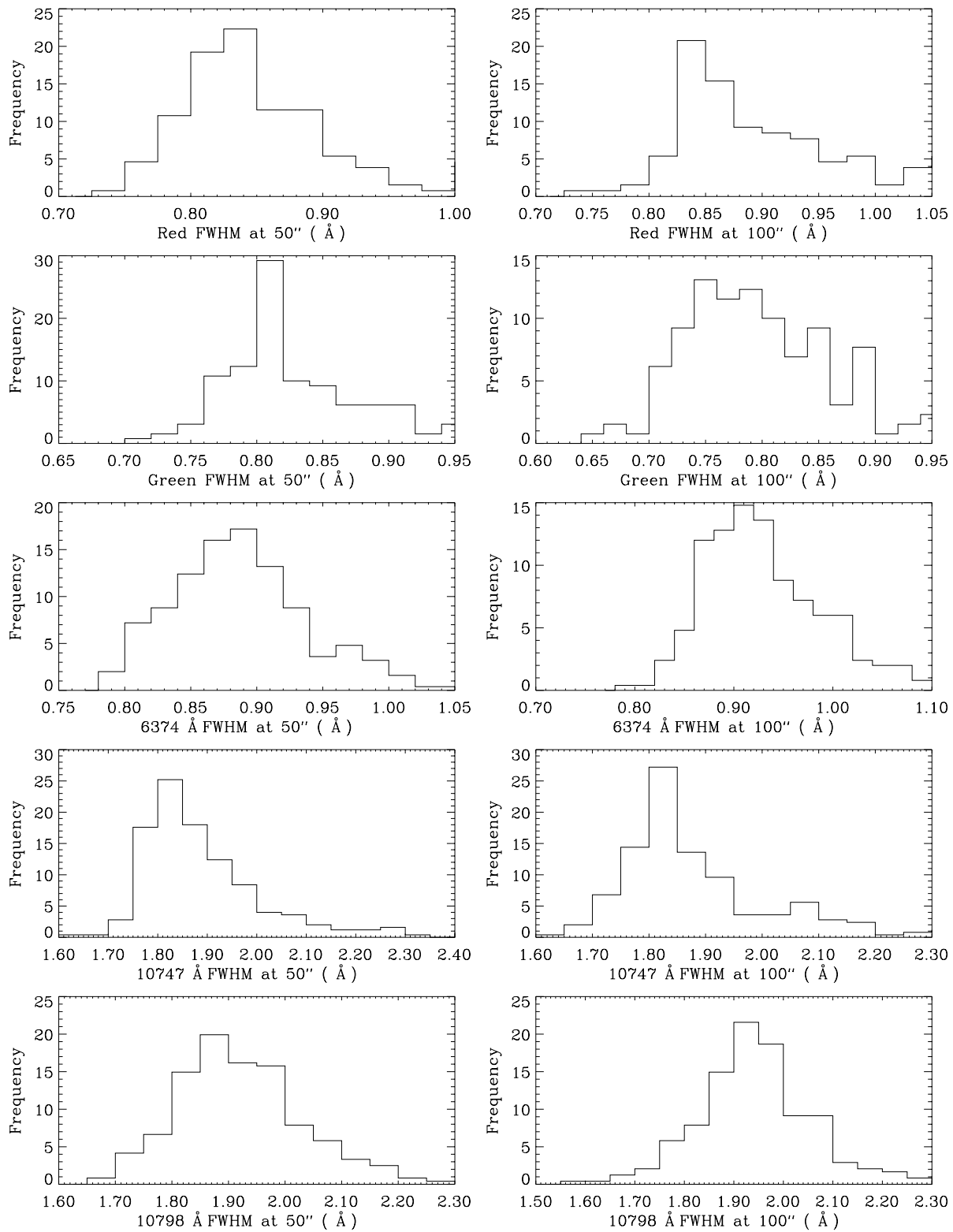


FIG. 5.—Frequency distribution of the FWHM at a height of 50'' and 100'' for simultaneous observations in the red and green lines is shown in the top four panels, and that of the red and infrared observations on some other days is plotted in the bottom six panels.

the red line. This difference may be due to the fact that their value is based on a single observation, whereas ours is the average over large number of observations obtained on several days, or the difference may be caused by a small difference in the ionization temperatures for these two ions. Doyle, Banerjee, & Perez (1998) interpreted the observed

increase in the line width as the increase in nonthermal velocity from $\approx 24 \text{ km s}^{-1}$ at the limb to $\approx 28 \text{ km s}^{-1}$ at 35'' above the limb for a plasma of around $0.8 \times 10^6 \text{ K}$. These values are larger than the average value of nonthermal velocity ($\approx 15 \text{ km s}^{-1}$) for the red line we observed. Seely et al. (1997) raised doubt about the commonly made

assumption of ion temperature being comparable to the electron temperature for the ionization equilibrium. They argued that if the ion temperature were to increase above the limb, then this could produce the observed line widths without necessarily implying an increase in the nonthermal velocity. Recently, Doschek et al. (2001), from the observations in polar coronal holes, found that the FWHM of the lines generally increases with height, though in some cases the increase is only marginal.

The average values of the FWHM gradients for the Fe XIV, Fe XIII, and Fe X coronal emission lines, and the associated temperatures of maximum fractional abundance of their ions for these lines, indicate that both of these parameters are inversely correlated. The increase in FWHM with height for a coronal emission line depends upon its ionization temperature. We speculate that the FWHM of the emission lines in coronal structures increases with height if the ionization temperature of the ion involved is less than 1.6×10^6 K, and decrease for those greater than 1.6×10^6 K. The amplitude of variation is dependent upon the ionization temperature of the line, since the increase in FWHM with height for the Fe XIII lines representing a temperature of 1.6×10^6 K is marginal.

In summary, the observed height variations of the FWHM of the red, infrared, and green lines show that the ions creating these emission lines cannot share the same temperature and turbulent velocity. In other words, these lines cannot be emitted from the same volume of plasma, and an introduction of some kind of inhomogeneity is unavoidable. Furthermore, the turbulent velocity of the green line decreases with height unless we assume an unreasonable temperature decrease with height. Therefore, the behavior of the line width of the green line is unfavorable in attributing the turbulent broadening to waves propagating in the steady coronal structures.

It is possible to explain the anti-correlated behavior of the change in width with height of the red and green lines if we assume that the fine structures in the steady and quiet coronal structures, although they may be broadly guided by magnetic field configuration, are also due to temperature and density variations within the structures. At the bottom of a coronal structure, where the plasma density is high, and

perhaps the magnetic field is strong and more concentrated, the contribution to the red line emission comes from a relatively cold plasma and that to the green line from a relatively hot plasma. Infrared lines represent the plasma at a temperature in between that of the red and green lines. It is possible that the hotter plasma surrounds the cold plasma, since the structures seen in the green and infrared lines appear broad and diffused as compared to the structures seen in the red line. As we move up along the coronal structure, the magnetic field spreads, as indicated by the broadening of structures at larger heights above the limb, and some mixing of hotter and relatively colder plasma may occur due to the existence of large thermal and nonthermal velocities. The mixed plasma at larger heights may have an average temperature lower than that of the green line plasma and higher than that of the red line plasma at the bottom of the structure. This process can cause an increase in the FWHM of the red line and decrease in the green line FWHM with height in the coronal structures. This also supports the observed small variation in the FWHM of infrared lines with height. Similarly, the observed variation in FWHM with height in these coronal emission lines can also be explained in terms of changes in the nonthermal velocity with height above the limb.

6. CONCLUSION

The observed variation in the FWHM of the green, red, and infrared lines with height above the limb raises doubts about the wave heating mechanism in the steady emission line coronal structures. The observed behavior of variation of FWHM with height can be explained by assuming the mixing of plasma at higher altitudes in the coronal structures. It appears that the observed average FWHM gradients and the ionization temperature associated with these lines are inversely correlated.

Part of the work was done during the visit of J. S. to National Astronomical Observatory of Japan. J. S. thanks A. V. Raveendran, J. S. Nathan, and N. K. Pramila for their assistance in data reduction. We thank the referee for useful comments.

REFERENCES

- Arnaud, M., & Rothenflug, R. 1985, *A&AS*, 60, 425
 Doschek, G. A., & Feldman, U. 2000, *ApJ*, 529, 599
 Doschek, G. A., Feldman, U., Laming, J. M., Schuhle, U., & Wilhelm, K. 2001, *ApJ*, 546, 559
 Doschek, G. A., Feldman, U., VanHoosier, M. E., & Bartoe, J. D. F. 1976, *ApJS*, 31, 417
 Doyle, J. G., Banerjee, D., & Perez, M. E. 1998, *Sol. Phys.*, 181, 91
 Hara, H., & Ichimoto, K. 1999, *ApJ*, 513, 969
 Hassler, D. M., Rottman, G. J., Shoub, E. C., & Holzer, T. E. 1990, *ApJ*, 348, L77
 Mariska, J. T., Feldman, U., & Doschek, G. A. 1978, *ApJ*, 226, 698
 Raju, P. K., & Singh, J. 1987, *Sol. Phys.*, 110, 271
 Seely, J. F., Feldman, U., Schuhle, U., Wilhelm, K., Curdt, W., & Lemaire, P. 1997, *ApJ*, 484, L87
 Singh, J., Ichimoto, K., Imai, H., Sakurai, T., & Takeda, A. 1999, *PASJ*, 51, 269
 Singh, J., Sakurai, T., Ichimoto, K., Suematsu, Y., & Takeda, A. 2002a, *PASJ*, 54, 793
 Singh, J., Sakurai, T., Ichimoto, K., & Takeda, A. 2002b, *PASJ*, 54, 807